MITSUBISHI ELECTRIC RESEARCH LABORATORIES
https://www.merl.com

Distributed Radar Autofocus Imaging Using Deep Priors

Mansour, Hassan; Lohit, Suhas; Boufounos, Petros T.

TR2022-129 October 19, 2022

Abstract

Antenna position ambiguity is a common problem that affects radar imaging systems that are mounted on mobile platforms. Existing approaches that aim to recover a sharp radar image despite this ambiguity aim to estimate the shift in the antenna position by modeling the radar scene as a sparse image with a small number of tar- gets using explicit analytical models for the statistical distribution of the targets in a radar image. The radar imaging problem is then solved by alternating between estimating the radar image, followed by estimating the shift in the antenna positions, until convergence is reached. While such approaches have shown tremendous success, they still struggle to recover the true target positions and may arrive at incorrect local optima when the measurement noise level is high. In this work, we develop a data-driven learning-based strategy for modeling the image of the radar scene instead of relying on explicit analytical models. We adopt a residual Unet architecture of a neural network to act as a denoising operator which takes a backprojected radar image as input and outputs a true target image. While deep denoisers may generally result in unstable iterative algorithms, we introduce a simple filtering step that suppresses noise belonging to the null space of the radar operator from the iterates to stabilize the iterative procedure. We evaluate the effectiveness of our solution using simulated numerical experiments and demonstrate its superiority over the analytic signal prior.

IEEE International Conference on Image Processing (ICIP) 2022

Mitsubishi Electric Research Laboratories, Inc.
201 Broadway, Cambridge, Massachusetts 02139

DISTRIBUTED RADAR AUTOFOCUS IMAGING USING DEEP PRIORS

Hassan Mansour, Suhas Lohit, Petros T. Boufounos

Mitsubishi Electric Research Laboratories,
201 Broadway, Cambridge, MA 02139, USA
{mansour,slohit,petrosb}@merl.com

ABSTRACT

Antenna position ambiguity is a common problem that affects radar imaging systems that are mounted on mobile platforms. Existing approaches that aim to recover a sharp radar image despite this ambiguity aim to estimate the shift in the antenna position by modeling the radar scene as a sparse image with a small number of targets using explicit analytical models for the statistical distribution of the targets in a radar image. The radar imaging problem is then solved by alternating between estimating the radar image, followed by estimating the shift in the antenna positions, until convergence is reached. While such approaches have shown tremendous success, they still struggle to recover the true target positions and may arrive at incorrect local optima when the measurement noise level is high. In this work, we develop a data-driven learning-based strategy for modeling the image of the radar scene instead of relying on explicit analytical models. We adopt a residual Unet architecture of a neural network to act as a denoising operator which takes a backprojected radar image as input and outputs a true target image. While deep denoisers may generally result in unstable iterative algorithms, we introduce a simple filtering step that suppresses noise belonging to the null space of the radar operator from the iterates to stabilize the iterative procedure. We evaluate the effectiveness of our solution using simulated numerical experiments and demonstrate its superiority over the analytic signal prior.

***Index Terms*—** Radar autofocus, blind deconvolution, sparse image reconstruction, deep image priors, block-coordinate descent

1. INTRODUCTION

Distributed radar imaging has emerged in recent years as an essential tool in a variety of remote sensing applications that require high resolution imaging. By combining measurements from spatially distributed antennas with relatively small apertures, distributed imaging achieves a large physical aperture that enables generates a high cross-range (azimuth) resolution [1–4]. The multi-antenna setup offers the advantage of reducing operational and maintenance costs, and adds flexibility and robustness to sensor failures.

The radar imaging resolution can be significantly improved by leveraging prior knowledge of the structure of the scene along with synchronization of the antennas and exact knowledge of their positions. However, the true antenna positions are often inexactly known with the uncertainty spanning multiple wavelengths despite the use of advanced positioning and navigation systems, such as the global navigation satellite system (GPS/GNSS) and the inertial navigation system (INS). To remedy this problem, several solutions have been proposed in the literature to compensate for the antenna position errors [5–10]. In some cases, the underlying structure of the radar image, such as its sparsity and spatial distribution, is utilized to limit the solution space and produce higher quality reconstructions [11–19].

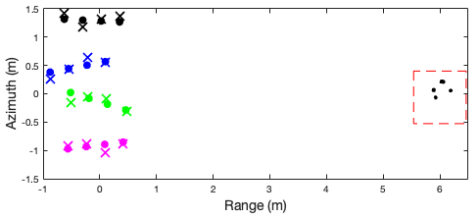

Fig. 1: A distributed radar acquisition system with position ambiguity. The round dots indicate the assumed but erroneous antenna positions, while the $\times$'s indicate the true positions.

In this paper, we explore the effectiveness of incorporating neural network-based denoisers as deep signal priors to replace the explicit analytical modeling of the spatial structure of a radar image in the distributed acquition setting. More formally, we are interested in the problem of recovering an image of a stationary scene composed of small number of targets, and represented in vector form as $\mathbf{x} \in \mathbb{C}^N$. The image is to be recovered by processing $F-$dimensional frequency-domain measurements $\{\tilde{\mathbf{y}}_m\}_{m=1}^M$ from M distributed antennas that suffer from position ambiguity. Following [18], we adopt the image domain convolution model to represent the radar perturbations. This model is exact in the colocated transmitter-receiver regime, which we also adopt in this paper. Let $\widetilde{\mathbf{A}}_m$ denote the radar propagation matrix at the *correct* antenna positions, and denote by $\mathbf{A}_m$ the corresponding matrix at the *incorrect* positions. Then the received radar measurements are given by $\tilde{\mathbf{y}}_m = \widetilde{\mathbf{A}}_m\mathbf{x} \neq \mathbf{A}_m\mathbf{x}$. Let $\mathbf{h}_m$ be a two-dimensional spatial shift kernel corresponding to the antenna perturbation, then we arrive at the image-domain convolution model represented as

$$\tilde{\mathbf{y}}_m = \mathbf{A}_m\left(\mathbf{x} * \mathbf{h}_m\right) + \mathbf{n}_m, \tag{1}$$

where the image $\mathbf{x}$ and the convolution kernels $\mathbf{h}_m$ are unknowns, and $\mathbf{n}_m$ denotes the measurement noise.

In [18, 19], a fused Lasso penalty function that combines the ℓ_1-norm with the total variation function was used to regularize the ill-posed inversion problem in (1) and promote sparsity along with piecewise smoothness of the reconstructed radar image. We explore a data-driven learning-based approach in this paper for modeling the image of the radar scene instead of relying on explicit analytical models. We adopt a residual Unet architecture of a neural network to act as a denoising operator that takes a backprojected radar image as input and outputs a true target image. However, incorporating such a neural network inside an iterative solver may result in an unstable

divergent algorithm. This divergent behavior results from the inability of the neural network to process noise belonging to the null-space of $\mathbf{A}$ that arises from iterative updates of the radar image since the network does not observe such noise during training. To remedy this divergent behavior, we introduce a module that filters out components belonging to the null-space of $\mathbf{A}$ from the iterates of $\mathbf{x}$ before applying the neural network denoiser. As a result, the incorporation of the deep denoiser inside the iterative solver becomes stable.

Over the past several years, a rich literature has emerged for incorporating deep signal priors within iterative reconstruction algorithms. In particular, the plug-and-play priors (PnP) [20] and the regularization-by-denoising (RED) [21, 22] frameworks replace explicit proximal mapping operators of penalty functions with sophisticated or learning-based denoisers to improve the reconstruction performance [23]. These deep prior based iterative methods have been proven to converge when the denoiser is properly trained to be non-expansive (or demi-contractive) [24,25]. While the above techniques have been shown to be quite effective at reconstructing signals while remaining relatively agnostic to the forward operator, it was shown that incorporating knowledge of the forward operator in the inversion process through algorithm unfolding or deep equilibrium architectures can significantly improve the reconstruction quality [26,27]. In the context of radar autofocus problems, deep denoisers have been proposed in the literature as part algorithm unfolding where the network learns to correct the phase of the iterates of the reconstructed image [28]. Other works considered the autofocus problem synthentic aperture sonar imaging as a postprocessing step where a deep denoiser was employed to correct the phase of the reconstructed image and reduce the computational time [29].

We describe in Section 2 the problem setup where we formalize the reconstruction problem and describe the general block-coordinate descent algorithm for solving the sparse blind deconvolution problem in the image domain. In Section 3, we present our proposed autofocus algorithm that exploits a deep image prior and discuss the stability of the proposed framework. Finally, we present numerical simulations in Section 4 that demonstrate the improvement in performance of the deep prior over the state-of-the-art analytical model, and conclude the paper in Section 5.

2. PROBLEM FORMULATION

2.1. Signal model

Consider a two-dimensional radar imaging scenario in which M distributed antennas are used to detect K targets. The targets are located within a spatial region of interest that is discretized on a grid $\Omega \subset \mathbb{R}^2, |\Omega| = N$, and $N = N_x \times N_y$ with N_x and N_y specifying the number of grid points in the horizontal and vertical directions.

Let $\Gamma \subset \mathbb{R}^2, |\Gamma| = M$ be the set of all the spatial locations of the M antennas. We consider the monostatic case where every antenna acts as a transmitter and receiver. A transmitting antenna at position $\boldsymbol{r} \in \Gamma$ emits a time-domain pulse $p(t)$ with frequency spectrum $P(\omega)$, where $\omega = 2\pi f$ is the angular frequency and $f \in \mathcal{B}$ is the ordinary frequency in the signal bandwidth $\mathcal{B}, |\mathcal{B}| = F$.

Denote by $\mathbf{y}_m$ and $\mathbf{A}_m$ the corresponding measurement vector and imaging operator of antenna pair indexed by m. Let $\tilde{\boldsymbol{r}}_m = \boldsymbol{r}_m + \boldsymbol{e}_m$ be the perturbed antenna positions, where $\boldsymbol{e}_m$ denotes the positioning errors. The receiver measurement $\tilde{\mathbf{y}}_m$ observes the scene reflectivity $\mathbf{x}$ through the perturbed imaging operator $\widetilde{\mathbf{A}}_m$, i.e.,

$$\tilde{\mathbf{y}}_m = \widetilde{\mathbf{A}}_m \mathbf{x} + \mathbf{n}_m. \tag{2}$$

Since the operator $\widetilde{\mathbf{A}}_m$ is unknown, we need to define the received measurements $\tilde{\mathbf{y}}_m$ as a function of $\mathbf{A}_m$ and $\mathbf{x}$. Let $\mathbf{h}_m \in \mathbb{R}^{N_h^2}, N_h \leq \min\{N_x, N_y\}$ be a vectorized two-dimensional shift kernel of size $N_h \times N_h$. Under the image domain convolutional model, the received signal of the antenna pair indexed by m is written as in (1).

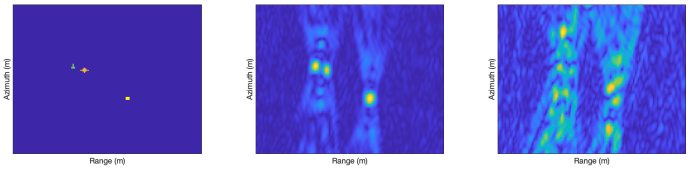

(a) (b) (c)

Fig. 2: Example of the iteration noise that is generated for (a) a target scene, (b) the first iteration given the radar operator corresponding to the true antenna positions, and (c) the first iteration given the radar operator corresponding to the incorrect antenna positions.

2.2. Reconstruction problem

Consider the image-domain convolution model expressed in the spatial Fourier domain below

$$\begin{aligned} \tilde{\mathbf{y}}_m &= \mathbf{A}_m (\mathbf{x} * \mathbf{h}_m) + \mathbf{n}_m \\ &= \mathbf{A}_m \mathbf{F}_2^{\mathsf{H}} \mathbf{D}_{\hat{\mathbf{h}}_m} \hat{\mathbf{x}} + \mathbf{n}_m, \end{aligned} \tag{3}$$

where $\mathbf{F}_2$ is the two dimensional Fourier transform operator applied to the vectorization of a matrix, $\hat{\mathbf{h}}_m = \mathbf{F}_2 \mathbf{h}_m$ and $\hat{\mathbf{x}} = \mathbf{F}_2 \mathbf{x}$ denote the two-dimensional Fourier transforms of $\mathbf{h}_m$ and $\mathbf{x}$, respectively, and $\mathbf{D}_{\hat{\mathbf{h}}_m}$ is the diagonal matrix with $\hat{\mathbf{h}}_m$ on the diagonal.

We define the regularized inversion problem for computing the radar reflectivity image $\mathbf{x}$ and the spatial convolution filters $\mathbf{h}_m$ from noisy measurements $\tilde{\mathbf{y}}_m$ as follows:

$$\begin{aligned} \min_{\substack{\mathbf{x} \in \mathbb{C}^N, \\ \mathbf{h}_m \in \mathbb{R}_+^{N_h^2}}} \quad & \sum_{m=1}^{M} \tfrac{1}{2} \|\tilde{\mathbf{y}}_m - \mathbf{A}_m \mathbf{F}_2^{\mathsf{H}} \mathbf{D}_{\hat{\mathbf{h}}_m} \hat{\mathbf{x}}\|_2^2 \\ \text{subject to} \quad & \mathbf{1}^T \mathbf{h}_m = 1, \forall\, m \in \{1 \dots M\}, \\ & \boldsymbol{R}_{\mathbf{x}}(\mathbf{x}) \leq 0 \end{aligned} \tag{4}$$

where $\boldsymbol{R}_{\mathbf{x}}(\cdot)$ is a penalty function for $\mathbf{x}$, and $\mathbf{1}$ is the all one vector. In [18, 19], a fused Lasso penalty [30] was used to regularize the ill-posedness of the problem in (4). We will describe below our proposed deep prior based implicit regularization approach that replaces the explicit prior.

3. RADAR AUTOFOCUS USING DEEP PRIORS

3.1. Deep denoiser as a mapping function

Deep signal priors have recently been shown to offer a significant boost to the signal reconstruction quality in a wide range of applications. One approach for incorporating the deep prior in the solution to an inverse problem is to train a deep denoiser to replace the proximal mapping operator or the projector onto the class of desirable signals with the deep denoiser.

Unlike the plug-and-play approaches [20–23], we emphasize here the importance of *not* using a Gaussian denoiser since the iterates generated during the inversion process exhibit artifacts that are far from additive white Guassian noise. This phenomenon is illustrate in Figure 2. To that effect, we train a deep denoiser $\mathcal{D}_\theta(\cdot)$

that can map from the space of backprojected images to the space of ground truth images. Specifically, for a set of radar measurements $\mathbf{y} = \mathbf{A}\mathbf{x} + \mathbf{n}$, we have:

$$\mathcal{D}_\theta(\mathbf{A}^{\mathsf{H}}\mathbf{y}) : \mathbf{A}^{\mathsf{H}}\mathbf{y} \to \mathbf{x}, \tag{5}$$

where the vector θ denotes the trainable neural network parameters. Given a training set of target radar images $\mathbf{x} \in \mathcal{X}$ with associated radar operators and noisy measurements $\mathbf{y} = \mathbf{A}\mathbf{x} + \mathbf{n}$, the training procedure then optimizes for the parameters θ by minimizing the mean square error loss as follows:

$$\theta^* = \arg\min_\theta \|\mathbf{x} - \mathcal{D}_\theta(\mathbf{A}^{\mathsf{H}}\mathbf{y})\|_2^2, \ \forall \mathbf{x} \in \mathcal{X}. \tag{6}$$

This approach is similar in spirit to algorithm unfolding and deep equilibrium architectures in that the denoiser is provided with examples of the noise that arises in the iterative updates. The difference is that our approach much simpler train and requires far less memory during the training process. The caveat is that an algorithm that incorporates such a denoiser quickly becomes unstable since the denoiser is not trained on noise experienced in later iterations.

3.2. Stabilizing the deep denoiser

To illustrate the effect of iteration noise, we consider a forward-backward splitting (FBS) procedure, such as the proximal gradient descent (PGD) iteration, with the proximal mapping operation replaced by the deep denoiser, i.e.,

$$\mathbf{x}^{t+1} = \mathcal{D}\left((\mathbf{I} - \alpha\mathbf{A}^{\mathsf{H}}\mathbf{A})\mathbf{x}^t + \alpha\mathbf{A}^{\mathsf{H}}\mathbf{y}\right). \tag{7}$$

Next, we note that the training procedure of our deep denoiser is identical to the first PGD iteration with zero initialization and is given by

$$\begin{aligned} \mathbf{x}^1 &= \mathcal{D}\left(\alpha\mathbf{A}^{\mathsf{H}}(\mathbf{A}\mathbf{x}^* + \mathbf{n})\right) \\ &= \mathbf{x}^* + \mathbf{e}^1, \end{aligned} \tag{8}$$

where $\mathbf{x}^*$ is the target signal, and $\mathbf{e}^1$ denotes the noise vector of the first iteration that contains elements from the null space of $\mathbf{A}$. Applying the same procedure to later iterations results in the following expression after rearranging some terms:

$$\mathbf{x}^t = \mathcal{D}\left(\mathbf{x}^* + \alpha\mathbf{A}^{\mathsf{H}}(\mathbf{n} - \mathbf{A}\mathbf{n}^{t-1}) + \mathbf{e}^{t-1}\right), \tag{9}$$

where $\mathbf{e}^{t-1}$ is the noise term from iteration $t-1$ that also contains components from the null space of $\mathbf{A}$.

However, our denoiser training procedure does not provide the denoiser with examples of noise outside of the range space of $\mathbf{A}$. Therefore, we propose to add a filtering step to suppress the null space components by multiplying the iterates by $\mathbf{A}^{\mathsf{H}}\mathbf{A}$ before inputting into the denoiser, i.e.:

$$\mathbf{x}^t = \mathcal{D}\left(\mathbf{A}^{\mathsf{H}}\mathbf{A}\left(\mathbf{x}^* + \alpha\mathbf{A}^{\mathsf{H}}(\mathbf{e} - \mathbf{A}\mathbf{n}^{t-1}) + \mathbf{n}^{t-1}\right)\right). \tag{10}$$

We observed that using such a simple filtering step stabilizes the iterative process and results in convergent algorithms without imposing any Lipschitz constraints on the structure of the network.

3.3. Reconstruction algorithm

It is evident from (4) that the overall problem is nonconvex and our aim is to find a stationary point to the problem. Therefore, we follow a block coordinate descent approach, summarized in Algorithm 1, that alternates between the accelerated projected gradient `apg` subroutine in Algorithm 2 and the forward backward splitting `fbs` subroutine in Algorithm 3 for each of $\mathbf{h}_m$, and $\mathbf{x}$, respectively. We define the forward operator of the image $\mathbf{x}$ for a fixed $\mathbf{h}_m^t$ at iteration t as

$$\mathcal{A}_{\mathbf{x}}^m(\mathbf{h}_m^t) := \mathbf{A}_m\mathbf{F}_2^{\mathsf{H}}\mathbf{D}_{\mathbf{F}_2\mathbf{h}_m^t}\mathbf{F}_2. \tag{11}$$

Similarly, the forward operator of the shift kernel $\mathbf{h}_m$ for a fixed $\mathbf{x}^t$ at iteration t is defined as

$$\mathcal{A}_{\mathbf{h}}^m(\mathbf{x}^t) := \mathbf{A}_m\mathbf{F}_2^{\mathsf{H}}\mathbf{D}_{\mathbf{F}_2\mathbf{x}^t}\mathbf{F}_2. \tag{12}$$

The shift kernels $\mathbf{h}_m$ are all initialized to the no-shift kernel $\mathbf{h}^0$, an $N_h \times N_h$ zero-valued matrix with the central entry set equal to one. For each descent step updating $\mathbf{h}_m$, we apply a small number of iterations of Nesterov's accelerated projected gradient descent (APG). Note that, every descent step of $\mathbf{h}_m$, produces an estimate $\tilde{\mathbf{h}}_m$ which does not necessarily satisfy the shift kernel properties, since we only run a small number of APG iterations. Therefore, we use a projector $\boldsymbol{P}(\tilde{\mathbf{h}}_m)$ onto the space of shift kernels which sparsifies $\tilde{\mathbf{h}}_m$ by setting its largest entry that is closest to the center to one and setting the remaining entries to zero. For the update of the image $\mathbf{x}$, we use a forward backward splitting approach where forward step minimizes the data mismatch and the backward step applies the deep denoiser to project the iterate on to the class of signals used in the training dataset.

Algorithm 1 Block coordinate descent for solving (4)

input: measurements $\{\tilde{\mathbf{y}}_m\}_{m=1}^M$, initial guess $\mathbf{x}^0$, $\mathbf{h}^0$, and maximum subroutine iterations T.
set: $j \leftarrow 1$; $\tilde{\mathbf{h}}_m^0, \mathbf{h}_m^0 \leftarrow \mathbf{h}^0$ for all m
repeat
  $\mathcal{A}_{\mathbf{x}}^m \leftarrow \mathcal{A}_{\mathbf{x}}^m(\mathbf{h}_m^{j-1})$ for all m
  $\mathbf{x}^j \leftarrow \texttt{fbs}(\{\mathcal{A}_{\mathbf{x}}^m\}_{m=1}^M, \lambda\boldsymbol{R}_{\mathbf{x}}, \{\tilde{\mathbf{y}}_m\}_{m=1}^M, \mathbf{x}^{j-1}, T)$
  for $m \leftarrow 1$ to M **do**
    $\mathcal{A}_{\mathbf{h}}^m \leftarrow \mathcal{A}_{\mathbf{h}}^m(\mathbf{x}^j)$
    $\tilde{\mathbf{h}}_m^j \leftarrow \texttt{apg}(\mathcal{A}_{\mathbf{h}}^m, \mu\boldsymbol{R}_{\mathbf{h}}, \tilde{\mathbf{y}}_m, \tilde{\mathbf{h}}_m^{j-1}, T)$
    $\mathbf{h}_m^j \leftarrow \boldsymbol{P}(\tilde{\mathbf{h}}_m^j)$
  $j \leftarrow j + 1$
until stopping criterion
return: estimate of the radar image $\mathbf{x}^j$.

Algorithm 2 `apg` subroutine for updating $\mathbf{h}_m$

input: $\mathcal{A}_{\mathbf{h}}^m, \mu\boldsymbol{R}_{\mathbf{h}}, \tilde{\mathbf{y}}_m, \tilde{\mathbf{h}}_m^{j-1}, T$.
set: $q_0 = 1$, $\mathrm{u}^0 = \mathrm{s}^0 = \tilde{\mathbf{h}}_m^{j-1}$
$\alpha \leftarrow$ inverse of maximum eigenvalue of $\mathcal{A}_{\mathbf{h}}^{m\mathsf{H}}\mathcal{A}_{\mathbf{h}}^m$
for $t \leftarrow 1$ to T **do**
  $\mathrm{z}^t \leftarrow \left(s^{t-1} + \alpha\mathcal{A}_{\mathbf{h}}^{m\mathsf{H}}\left(\tilde{\mathbf{y}}_m - \mathcal{A}_{\mathbf{h}}^m\,\mathrm{s}^{t-1}\right)\right)\Big|_{\mathbb{R}^+}$
  $\mathrm{u}^t \leftarrow \frac{1}{\mathbf{1}^T\,\mathrm{u}^t}\,\mathrm{u}^t$
  $q_t \leftarrow \frac{1+\sqrt{1+4q_{t-1}^2}}{2}$
  $\mathrm{s}^t \leftarrow \mathrm{u}^t + \frac{q_{t-1}-1}{q_t}(\,\mathrm{u}^t - \,\mathrm{u}^{t-1})$
return: s^T.

4. PERFORMANCE EVALUATION

We evaluate the performance of our radar autofocus framework using the simulation setup shown in Figure 1. The figure illustrates

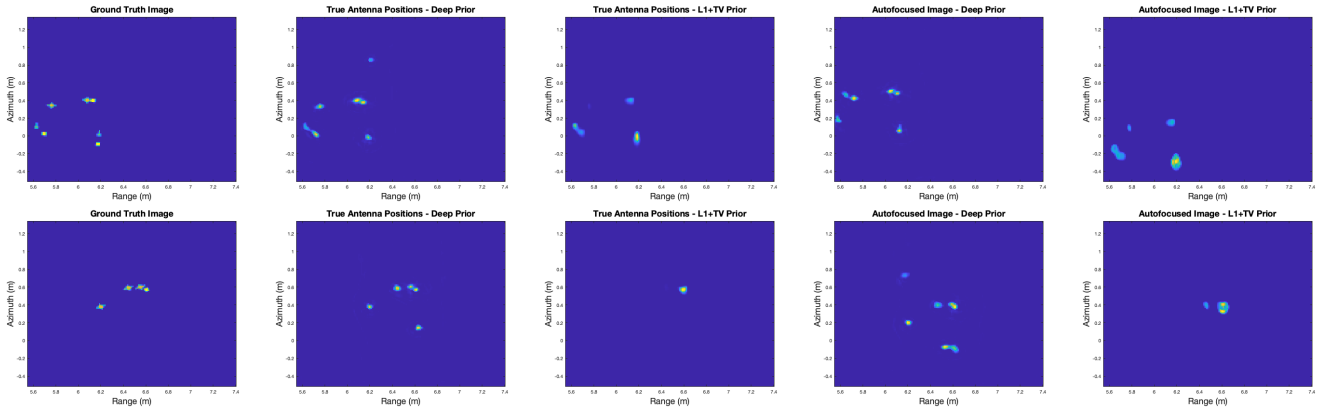

(a) (b) (c) (d) (e)

Fig. 3: Reconstructions for two example radar scenes at 20dB PSNR. The columns illustrate (a) the ground truth images, (b) reconstruction using the correct radar operator and deep prior, (c) the correct radar operator and fused Lasso penalty, (d) autofocus from the incorrect forward operator with the deep prior, and (e) autofocus from the incorrect radar operator with the fused Lasso penalty [18, 19].

Algorithm 3 `fbs` subroutine for updating $\mathbf{x}$

input: $\{\mathcal{A}_{\mathbf{x}}^m\}_{m=1}^M, \lambda \boldsymbol{R}_{\mathbf{x}}, \{\tilde{\mathbf{y}}_m\}_{m=1}^M, \mathbf{x}^{j-1}, T.$

set: $q_0 = 1,\ \mathrm{s}^0 = \mathbf{x}^{j-1}$

$\alpha \leftarrow$ inverse of maximum eigenvalue of $\sum_{m=1}^{M} \mathcal{A}_{\mathbf{x}}^{m\mathsf{H}} \mathcal{A}_{\mathbf{x}}^m$

for $t \leftarrow 1$ to T **do**

$\quad \mathrm{z}^t \leftarrow \mathrm{s}^{t-1} + \alpha \sum_{m=1}^{M} \mathcal{A}_{\mathbf{x}}^{m\mathsf{H}} \left(\tilde{\mathbf{y}}_m - \mathcal{A}_{\mathbf{x}}^m \mathrm{s}^{t-1}\right)$

$\quad \mathrm{v}^t \leftarrow \alpha \sum_{m=1}^{M} \mathcal{A}_{\mathbf{x}}^{m\mathsf{H}} \mathcal{A}_{\mathbf{x}}^m \mathrm{z}^t$

$\quad \mathrm{s}^t \leftarrow \mathcal{D}_{\theta^*}\left(\mathrm{v}^t\right)$

return: s^T.

a radar scene acquired by 16 distributed antennas divided into four arrays with average position error around 2λ and maximum error at 3.5λ, where λ is the wavelength of the center frequency of a differential Gaussian pulse centered at 6 GHz with a 9 GHz bandwidth. The true antenna positions are indicated by the $\times$'s whereas the erroneous assumed positions are indicated by the dots. The received signals are contaminated with white Gaussian noise at peak signal to noise ratios (PSNR) in the set $\{20, 10, 4\}$dB after matched-filtering with the transmitted pulse.

For training the denoiser, we generate a dataset composed of 7200 samples with the 100 distinct target configurations representing the ground truth images. For each distinct target configuration, we apply a random rotation and shift and we simulate radar measurements from 4 distributed arrays with a random number of antennas $M \in \{4, 8, 12, 16, 20, 24\}$. We then add Gaussian random noise to the radar measurements with target PSNR in the set $\{4, 6, 8, 10, 15, 20\}$. The noisy inputs to the deep denoiser are then generated by computing backprojected images using both the true and incorrect radar operators. The training dataset is then split (80/10/10) into 5760 training images, 720 validation images, and 720 test images.

Figure 3 shows a comparison between the reconstructed images obtained using the deep prior compared to using a fused Lasso penalty as in [18, 19]. It can be seen from the figure that even in the case of full antenna position knowledge, the deep prior does a better job at recovering the target image compared to the fused Lasso prior. Similarly, we observe superior performance when the autofocus algorithm is used. In both cases, there remains a global shift ambiguity due to the image-domain convolution model. Next, we compare the detection accuracy of the two prior models under different measurement PSNR values. Figure 4 shows the receiver operating characteristic (ROC) curves computed for twenty different target configurations. The figure illustrates that the deep prior model delivers comparable behavior to the fused Lasso prior at 10dB PSNR but significantly outperforms the analytical model in the 20dB and 4dB settings.

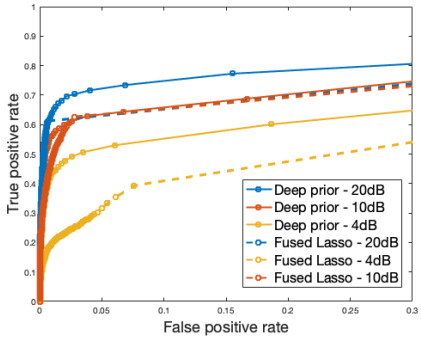

Fig. 4: ROC curves of the reconstructed images using the deep priors based scheme and the fused Lasso regularized scheme.

5. CONCLUSION

In conclusion, we presented a stable deep prior training approach for radar autofocus imaging that outperforms the fused Lasso prior. The algorithm stability depended on filtering out the null space of the forward operator before applying the deep denoiser. For future work, we plan to compare the performance of our approach to deep denoisers trained using the deep equilibrium model as well as the iteration unfolding model.

6. REFERENCES

[1] M. A. Herman and T. Strohmer, "High-resolution radar via compressed sensing," *IEEE Transactions on Signal Processing*, vol. 57, no. 6, pp. 2275–2284, June 2009.

[2] Y. Yu, A. P. Petropulu, and H. V. Poor, "Mimo radar using compressive sampling," *IEEE Journal of Selected Topics in Signal Processing*, vol. 4, no. 1, pp. 146–163, Feb 2010.

[3] C. R. Berger and J. M. F. Moura, "Noncoherent compressive sensing with application to distributed radar," in *2011 45th Annual Conference on Information Sciences and Systems*, March 2011, pp. 1–6.

[4] D. Liu, U. S. Kamilov, and P. T. Boufounos, "Sparsity-driven distributed array imaging," in *2015 IEEE 6th International Workshop on Computational Advances in Multi-Sensor Adaptive Processing (CAMSAP)*, Dec 2015, pp. 441–444.

[5] D. E. Wahl, P. H. Eichel, D. C. Ghiglia, and C. V. Jakowatz, "Phase gradient autofocus-a robust tool for high resolution sar phase correction," *IEEE Transactions on Aerospace and Electronic Systems*, vol. 30, no. 3, pp. 827–835, Jul 1994.

[6] L. Xi, L. Guosui, and J. Ni, "Autofocusing of isar images based on entropy minimization," *IEEE Transactions on Aerospace and Electronic Systems*, vol. 35, no. 4, pp. 1240–1252, Oct 1999.

[7] W. Ye, T. S. Yeo, and Z. Bao, "Weighted least-squares estimation of phase errors for sar/isar autofocus," *IEEE Transactions on Geoscience and Remote Sensing*, vol. 37, no. 5, pp. 2487–2494, Sep 1999.

[8] H. J. Cho and D. C. Munson, "Overcoming polar-format issues in multichannel sar autofocus," in *2008 42nd Asilomar Conference on Signals, Systems and Computers*, Oct 2008, pp. 523–527.

[9] K. H. Liu and D. C. Munson, "Fourier-domain multichannel autofocus for synthetic aperture radar," *IEEE Transactions on Image Processing*, vol. 20, no. 12, pp. 3544–3552, Dec 2011.

[10] M. P. Nguyen and S. B. Ammar, "Second order motion compensation for squinted spotlight synthetic aperture radar," in *Conference Proceedings of 2013 Asia-Pacific Conference on Synthetic Aperture Radar (APSAR)*, Sept 2013, pp. 202–205.

[11] N. O. Onhon and M. Cetin, "A sparsity-driven approach for joint sar imaging and phase error correction," *IEEE Transactions on Image Processing*, vol. 21, no. 4, pp. 2075–2088, April 2012.

[12] X. Du, C. Duan, and W. Hu, "Sparse representation based autofocusing technique for isar images," *IEEE Transactions on Geoscience and Remote Sensing*, vol. 51, no. 3, pp. 1826–1835, March 2013.

[13] S. Kelly, M. Yaghoobi, and M. Davies, "Sparsity-based autofocus for undersampled synthetic aperture radar," *IEEE Transactions on Aerospace and Electronic Systems*, vol. 50, no. 2, pp. 972–986, April 2014.

[14] J. Yang, X. Huang, J. Thompson, T. Jin, and Z. Zhou, "Compressed sensing radar imaging with compensation of observation position error," *IEEE Transactions on Geoscience and Remote Sensing*, vol. 52, no. 8, pp. 4608–4620, Aug 2014.

[15] D. Liu, U. S. Kamilov, and P. T. Boufounos, "Coherent distributed array imaging under unknown position perturbations," in *4th International Workshop on Compressed Sensing Theory and its Applications to Radar, Sonar and Remote Sensing (CoSeRa)*, Sept 2016, pp. 105–109.

[16] L. Zhao, L. Wang, G. Bi, S. Li, L. Yang, and H. Zhang, "Structured sparsity-driven autofocus algorithm for high-resolution radar imagery," *Signal Processing*, vol. 125, pp. 376 – 388, 2016.

[17] M. J. Hasankhan, S. Samadi, and M. Çetin, "Sparse representation-based algorithm for joint sar image formation and autofocus," *Signal, Image and Video Processing*, vol. 11, no. 4, pp. 589–596, May 2017.

[18] H. Mansour, U. S. Kamilov, D. Liu, and P. T. Boufounos, "Radar autofocus using sparse blind deconvolution," in *IEEE International Conference on Acoustics, Speech, and Signal Processing (ICASSP)*, Apr. 2018, pp. 1623–1627. [Online]. Available: https://www.merl.com/publications/TR2018-003

[19] H. Mansour, D. Liu, U. Kamilov, and P. T. Boufounos, "Sparse blind deconvolution for distributed radar autofocus imaging," *IEEE Transactions on Computational Imaging*, vol. 4, no. 4, pp. 537–551, Dec. 2018. [Online]. Available: https://www.merl.com/publications/TR2018-179

[20] S. V. Venkatakrishnan, C. A. Bouman, and B. Wohlberg, "Plug-and-play priors for model based reconstruction," in *IEEE Global Conference on Signal and Information Processing*, 2013, pp. 945–948.

[21] Y. Romano, M. Elad, and P. Milanfar, "The little engine that could: Regularization by denoising (red)," *SIAM Journal on Imaging Sciences*, vol. 10, no. 4, pp. 1804–1844, 2017.

[22] E. T. Reehorst and P. Schniter, "Regularization by denoising: Clarifications and new interpretations," *IEEE Transactions on Computational Imaging*, vol. 5, no. 1, pp. 52–67, 2019.

[23] C. A. Metzler, A. Maleki, and R. G. Baraniuk, "From denoising to compressed sensing," *IEEE Transactions on Information Theory*, vol. 62, no. 9, pp. 5117–5144, 2016.

[24] E. Ryu, J. Liu, S. Wang, X. Chen, Z. Wang, and W. Yin, "Plug-and-play methods provably converge with properly trained denoisers," in *Proceedings of the 36th International Conference on Machine Learning*, ser. Proceedings of Machine Learning Research, K. Chaudhuri and R. Salakhutdinov, Eds., vol. 97. PMLR, 09–15 Jun 2019, pp. 5546–5557.

[25] R. Cohen, M. Elad, and P. Milanfar, "Regularization by denoising via fixed-point projection (red-pro)," *SIAM Journal on Imaging Sciences*, vol. 14, no. 3, pp. 1374–1406, 2021.

[26] K. Zhang, W. Zuo, S. Gu, and L. Zhang, "Learning deep cnn denoiser prior for image restoration," in *IEEE Conference on Computer Vision and Pattern Recognition (CVPR)*, 2017, pp. 2808–2817.

[27] D. Gilton, G. Ongie, and R. Willett, "Deep equilibrium architectures for inverse problems in imaging," 2021.

[28] E. Mason, B. Yonel, and B. Yazici, "Deep learning for radar," in *IEEE Radar Conference (RadarConf)*, 2017, pp. 1703–1708.

[29] I. D. Gerg and V. Monga, "Real-time, deep synthetic aperture sonar (sas) autofocus," in *IEEE International Geoscience and Remote Sensing Symposium IGARSS*, 2021, pp. 8684–8687.

[30] R. Tibshirani, M. Saunders, S. Rosset, J. Zhu, and K. Knight, "Sparsity and smoothness via the fused lasso," *Journal of the Royal Statistical Society: Series B (Statistical Methodology)*, vol. 67, no. 1, pp. 91–108, 2005.